Tellus (2000), 52B, 636–651
Printed in UK. All rights reserved

TELLUS
ISSN 0280–6509

Ground-based lidar measurements of aerosols during ACE-2: instrument description, results, and comparisons with other ground-based and airborne measurements

By ELLSWORTH J. WELTON[1]*, KENNETH J. VOSS[1], HOWARD R. GORDON[1], HAL MARING[2], ALEXANDER SMIRNOV[3], BRENT HOLBEN[3], BEAT SCHMID[4], JOHN M. LIVINGSTON[5], PHILIP B. RUSSELL[5], PHILIP A. DURKEE[6], PAOLA FORMENTI[7] and MEINRAT O. ANDREAE[7], [1]*University of Miami, Physics Department, 1320 Campo Sano Dr., Coral Gables, Fl 33143, USA;* [2]*RSMAS/MAC, University of Miami, 4600 Rickenbacker Causeway, Miami, Fl 33149, USA;* [3]*Science Systems and Applications, Inc., NASA-GSFC Code 923, Greenbelt, MD 20771, USA;* [4]*Bay Area Environmental Research Institute, NASA Ames Research Center, MS 245-5, Moffett Field, CA 94035-1000, USA;* [5]*SRI International, MS 245-5, NASA Ames Research Center, Moffett Field, CA 94035-1000, USA;* [6]*Meteorology Department, Code MR/DE, Naval Postgraduate School, 589 Dyer Rd., Monterey, CA 93943-5114, USA;* [7]*Max Planck Institut fur Chemie, Biogeochemistry Department, PO Box 3060, 55020 Mainz, Germany*

(Manuscript received 1 February 1999; in final form 20 September 1999)

ABSTRACT

A micro-pulse lidar system (MPL) was used to measure the vertical and horizontal distribution of aerosols during the Aerosol Characterization Experiment 2 (ACE-2) in June and July of 1997. The MPL measurements were made at the Izaña observatory (IZO), a weather station located on a mountain ridge (28°18′ N, 16°30′ W, 2367 m asl) near the center of the island of Tenerife, Canary Islands. The MPL was used to acquire aerosol backscatter, extinction, and optical depth profiles for normal background periods and periods influenced by Saharan dust from North Africa. System tests and calibration procedures are discussed, and an analysis of aerosol optical profiles acquired during ACE-2 is presented. MPL data taken during normal IZO conditions (no dust) showed that upslope aerosols appeared during the day and dissipated at night and that the layers were mostly confined to altitudes a few hundred meters above IZO. MPL data taken during a Saharan dust episode on 17 July showed that peak aerosol extinction values were an order of magnitude greater than molecular scattering over IZO, and that the dust layers extended to 5 km asl. The value of the dust backscatter–extinction ratio was determined to be $0.027 \pm 0.007\ \mathrm{sr}^{-1}$. Comparisons of the MPL data with data from other co-located instruments showed good agreement during the dust episode.

1. Introduction

The Aerosol Characterization Experiment 2 (ACE-2) ran from 16 June 1997 to 25 July 1997. The purpose of ACE-2 was to study the radiative properties and physical characteristics of anthropogenic aerosols from Europe, and dust aerosols from Africa, as they are transported across the North Atlantic Ocean. An overview of ACE-2 operations and specific activities can be found in Raes et al. (2000). One of the ACE-2 activities was the "clear sky column closure experiment" (CLEARCOLUMN), which was aimed at simul-

* Corresponding author. Present affiliation: Science Systems and Applications, Inc., NASA-GSFC Code 912, Greenbelt, MD 20771, USA.
e-mail: welton@virl.gsfc.nasa.gov

taneous measurements of aerosol properties using a variety of different platforms in order to assess the aerosol direct radiative forcing (Russell and Heintzenberg, 2000). The work presented in this paper was part of the CLEARCOLUMN effort during ACE-2.

This paper will focus on lidar measurements of the vertical and horizontal structure of aerosols surrounding the Izaña observatory (IZO) on Tenerife, Canary Islands during ACE-2. IZO is located on a mountain ridge (28°18′N, 16°30′W, 2367 m asl) near the center of the island and has often been used as a site for the study of various aerosol properties (Prospero et al., 1995; Raes et al., 1997; Smirnov et al., 1998). However, lidar measurements at IZO have not been made prior to this study. Lidar measurements can provide accurate knowledge of the spatial distribution of aerosols in the atmosphere surrounding IZO (10–30 km radius).

In addition to the lidar observations, in situ aerosol scattering, absorption, and mass concentration measurements were made at IZO. These in situ measurements were used to aid in the calibration of the lidar system (as described in Section 3), and in comparisons with the lidar data. Sunphotometer measurements were also made at IZO in order to supply spectral aerosol optical depth (AOD) measurements for CLEARCOLUMN efforts and for use in a lidar inversion algorithm (Section 7). The algorithm uses the sunphotometer AOD along with the lidar data to produce the columnar backscatter–extinction ratio, and profiles of the aerosol extinction coefficient and AOD. The lidar derived aerosol optical data were used to examine normal IZO site conditions (no dust), as well as conditions seen during Saharan dust passages. Finally, comparisons between the lidar data and data from other ACE-2 CLEARCOLUMN instruments are presented. In addition to daily comparisons with the other IZO instruments, joint measurements of AOD on the afternoon of 17 July 1997 dust episode were performed with the lidar, a sunphotometer on board an ACE-2 aircraft, and a radiometer installed on the nearby volcano of Tenerife (Teide). The comparisons demonstrate the success of the lidar calibration techniques and the lidar inversion algorithm, and show that lidar analysis can produce accurate profiles of ambient aerosol optical properties.

2. Instrumentation

2.1. Micro-pulse lidar system (MPL)

The lidar used in this study is a micro-pulse lidar system (MPL) manufactured by Science and Engineering Services Inc., USA. Basic MPL design and background is described in Spinhirne (1993) and Spinhirne et al. (1995). The MPL system is revolutionary in that it uses rapidly pulsed low intensity laser light. The MPL system has output energies at the μJ level, and the beam is expanded to 20.32 cm in diameter which achieves ANSI eye-safe standards. A pulse repetition frequency (PRF) of 2500 Hz allows the system to average many low energy pulses in a short time to achieve a good signal-to-noise ratio. In practice, an averaging time of 1 min is used for data collection but the stored signals can be averaged over longer periods if necessary during post-analysis. The MPL system also has a high vertical spatial resolution (30–75 m). Finally, the MPL system is small compared to previous lidar systems and is therefore much more portable than its predecessors. The small size of the MPL system allows the operator to perform lidar measurements at any zenith angle by tilting the instrument to the desired angle. It is therefore possible to perform horizontal and slant path measurements with the MPL as well as the normal vertical measurements. Care must be taken when operating the MPL during sunny days as direct sunlight entering the MPL can cause serious damage to the detector. The MPL must be tilted away from the sun or turned off and covered in such conditions.

The MPL is pictured schematically in Fig. 1. The MPL transmitter–receiver (T–R) is located inside the climate housing and consists of a black 20.32 cm diameter Cassegrain telescope with optics and electronics mounted directly below the telescope. The laser supply and scalar (data binning unit) are connected to the T–R, and along with the control computer, they must be located inside a separate climate controlled environment. The laser supply contains a diode pumped Nd:YLF laser with a fundamental pulse output wavelength of 1046 nm that is converted to 523 nm for lidar use after passage through a frequency doubling crystal. The MPL system used in this study was operated at the full laser power supply setting of 1 W. The pulse duration is 10 ns with a

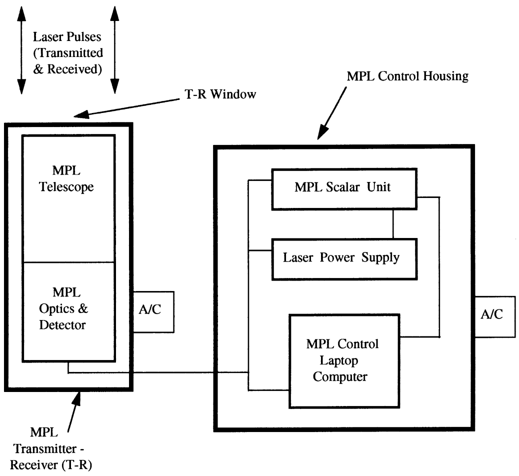

Fig. 1. Schematic diagram of the micro-pulse lidar system (not to scale).

PRF of 2500 Hz and output energies ranging from 1 to 6 μJ depending upon system performance. Signals are received using the same telescope and are recorded with a Geiger mode avalanche photodiode.

The signals are stored as photons/s (ph/s). Since the receiver is a telescope focused at infinity, the T–R has difficulty accurately imaging near-range signals onto the detector. This problem is referred to as overlap error and causes the near-range signals (0 to approximately 2 km) to rapidly fall off in intensity the closer they are to the T–R. Since the majority of aerosols are contained in the first several kilometers of the atmosphere (or as at IZO, the first several kilometers in range from IZO), the overlap problem must be overcome. The procedures used in this study to correct for the MPL overlap are discussed in Section 3. The signals are binned in the scalar according to their time-of-flight from transmission to signal reception and correspond to steps of 75 m in range. Our MPL system has a pause of approximately 1 μs from activation of the detector to emission of the laser pulse. Thus, we disregard the first 2 signal bins and re-zero the range such that the third signal bin represents the signal return from 75 m.

A control computer is connected to the scalar and is used to control lidar operation, to visualize real-time lidar output, and to store the resulting lidar data. The data are stored in 1 h binary files with each record containing a header followed by the signal in ph/s at the successive 75 m increments up to a preset range (30 km). The maximum MPL range having usable data typically varies from approximately 30 km at night to about 10 km during reasonably clear daytime conditions. The lidar signals stored on the control computer contain background noise from sunlight at 523 nm and another noise signal referred to as afterpulse. Afterpulse noise is due to the release of photoelectrons from the photodiode detector with time and is largely caused by turning on the detector prior to triggering the laser pulse. The afterpulse noise is often several orders of magnitude lower than signal returns for the first several kilometers of range, but is significant at longer ranges. Afterpulse noise must be corrected in post-analysis and the procedure is discussed in Section 3. Background sunlight noise is measured by the MPL in real time by measuring the detector signal after the maximum altitude signal (30 km) has arrived and before the next pulse is fired. This background signal is stored and used to correct the final signal by subtracting its value from each binned signal in post-analysis. The header information contains the time, output pulse energy, instrument temperatures, background sunlight energies, and information necessary for the operator to determine the altitude resolution used for each record in the data file.

2.2. *Other IZO instruments*

In situ aerosol measurements were made at IZO. Aerosol mass concentration measurements were made with a Rupprecht & Patashnick Model 1400a tapered element oscillating microbalance, absorption was measured with a radiance research particle/soot absorption photometer, and scattering was measured with 2 instruments: a TSI model 3563 integrating nephelometer, and a radiance research model M903 integrating nephelometer. The scattering and absorption measurements were used to determine aerosol extinction at 550 nm (the instrument's wavelengths). The IZO in situ measurements were used for MPL calibrations and in comparisons with the MPL. A NASA AERONET Cimel sunphotometer (Holben et al., 1998) was also operated at IZO for the duration of ACE-2. The Cimel was used to acquire independent measurements of AOD (Smirnov et al., 1998) for input to the lidar inversion algorithm (Section 7) and to perform aerosol measurements specific to AERONET and CLEARCOLUMN operations. Cimel AOD values reported in this study are for the lidar wavelength of 523 nm. The Cimel AOD at 523 nm was calculated using power law fits to the measured AOD.

2.3. *Airborne and Teide Instruments*

One of the aircraft participating in ACE-2 was the Center for Interdisciplinary Remotely Piloted Aircraft Studies (CIRPAS) Pelican aircraft. AOD measurements were made on-board the Pelican with the NASA Ames Airborne Tracking 14-channel Sunphotometer, AATS-14 (Schmid et al., this issue). AOD measurements were also made on the island's volcano, Teide (28°16′N, 16°36′W, 3570 m asl), during ACE-2 using a multi-filter rotating shadowband radiometer (MFR-7, Yankee Environmental Systems, Inc.) (Formenti et al., 2000). AOD data acquired with the AATS-14 (525 nm) and the MFR-7 shadowband (501 nm) are used in the comparison for 17 July 1997.

3. The lidar equation and MPL calibrations

3.1. *Vertical lidar measurements*

The basic lidar equation for returned signals (for vertically oriented lidar) is given by:

$$S_L(z) = \frac{CE}{(z - z_L)^2}[\beta_R(z) + \beta_A(z)] \times \exp\left[-2\int_{z_L}^{z} (\sigma_R(z') + \sigma_A(z'))\,dz'\right], \quad (1)$$

where $S_L(z)$ is the lidar signal at altitude z (m), C is the system constant (principally a function of the optics), E is the output energy in μJ, z_L is the lidar altitude (m), $\beta(z)$ and $\sigma(z)$ are the backscatter ($m^{-1}\,sr^{-1}$) and extinction (m^{-1}) coefficients respectively, the R subscript denotes a Rayleigh quantity (due to molecular scattering), and the A subscript denotes an aerosol quantity.

The backscatter coefficient is related to extinction by

$$\beta(z) = R(z)\sigma(z), \quad (2)$$

where $R(z)$ is the backscatter–extinction ratio with units of sr^{-1}. The aerosol backscatter–extinction ratio is considered to be constant for each profile in this study and is referred to as the columnar backscatter–extinction ratio, R_A.

It is useful to rewrite eq. (1) by multiplying by the range squared, $(z - z_L)^2$, to remove the range dependent fall off in the signal returns and to use R_R and R_A to rewrite the equation in terms of only the backscatter coefficient,

$$S_r(z) = CE[\beta_R(z) + \beta_A(z)] \times \exp\left[-\frac{2}{R_R}\int_{z_L}^{z} \beta_R(z')\,dz'\right] \times \exp\left[-\frac{2}{R_A}\int_{z_L}^{z} \beta_A(z')\,dz'\right], \quad (3)$$

where $S_r(z)$ is referred to as the range-corrected lidar signal. The lidar equation must be solved for the unknown aerosol quantities, $\beta_A(z)$, $\sigma_A(z)$, and R_A. The Rayleigh optical functions are constructed using data from Hansen and Travis (1974). The values of R_R and R_A used above are assumed to be constant with altitude. While R_R is constant, R_A may actually vary. Algorithms exist for lidar analysis using altitude dependent R_A values (Klett, 1985; Kovalev, 1993) but require additional assumptions or measurements of the vertical structure of the aerosol optical properties that were not possible for this work. The lidar inversion algorithm in this study uses an independent AOD measurement to iterate a basic lidar inversion (Fernald et al., 1984) to produce the $\beta_A(z)$ and $\sigma_A(z)$ profiles, and to calculate the value of R_A. The lidar inversion algorithm used in this study is discussed in Section 7. Error related to assuming a constant R_A is also addressed in Section 7.

3.2. *Horizontal lidar measurements*

Horizontal lidar measurements are used to assess the horizontal homogeneity of the atmosphere at a particular altitude. The backscatter and extinction coefficients for a horizontal lidar measurement during conditions of horizontal homogeneity are constant by definition. Under this condition, a horizontal lidar signal is

$$S_H(x) = CE[\beta_R(z_L) + \beta_A(z_L)] \times \exp[-2(\sigma_R(z_L) + \sigma_A(z_L))x], \quad (4)$$

where $S_H(x)$ is the horizontal lidar signal, x is the horizontal range in meters, and the values of $\beta_i(z_L)$ and $\sigma_i(z_L)$ are constants with respect to x. Furthermore, taking the natural logarithm of both sides of eq. (4) gives

$$\ln[S_H(x)] = -2[\sigma_R(z_L) + \sigma_A(z_L)]x + \ln[CE(\beta_R(z_L) + \beta_A(z_L))]. \quad (5)$$

Thus, the slope of $\ln[S_H(x)]$ versus the range x yields $-2\sigma_{total}$ and the y-intercept is $\ln[CE\beta_{total}]$ during conditions of horizontal homogeneity. If the atmosphere is not horizontally homogeneous at the lidar altitude, then a horizontal lidar plot of $\ln[S_r(x)]$ versus the range x will not produce a straight line.

3.3. *MPL calibration procedure*

Eq. (3) is an ideal lidar signal. Actual lidar signals are effected by both afterpulse and overlap problems as mentioned in Section 2. Thus, an actual MPL range-corrected signal is given by

$$S_r(z) = \left\{ CO(z)E[\beta_R(z) + \beta_A(z)] \times \exp\left[-\frac{2}{R_R}\int_{z_L}^{z}\beta_R(z')\,dz'\right] \times \exp\left[-\frac{2}{R_A}\int_{z_L}^{z}\beta_A(z')\,dz'\right]\right\} + A(z), \quad (6)$$

where $O(z)$ and $A(z)$ represent the overlap and afterpulse functions.

Calibration of the MPL system involves correcting for the afterpulse and overlap functions and the determination of C. The calibration procedures applied to the MPL during ACE-2 differ from the normal MPL calibration techniques (Welton, 1998). The laser frequency doubling crystal in the MPL system burned midway through ACE-2. The cause of the burned crystal was attributed to a poor ground connection between the laser temperature controller on the laser supply and the laser itself, located inside the T–R. Data continued to be taken with the MPL system because the problem was not noticed until the end of the experiment.

The data acquired after the crystal burn had noticeable effects caused by signal loss and diffraction from the burn pattern. Signal loss resulted from light scattered off axis, by the hole, that was lost before reaching the T–R. Diffraction effects were believed to be the cause of distortions in the outgoing laser pulses. These diffraction effects caused distortion of the MPL overlap characteristics and altered the afterpulse signal. These problems became worse as the experiment continued. Thus it was not possible to use the pre-experiment calibrations or post-calibrations to correct the entire data set taken during the experiment. Therefore, a new lidar calibration procedure was developed to handle the MPL data during ACE-2. The procedure is based on normalization of the MPL signals to those signals from a molecular (Rayleigh) only atmosphere and is described below.

Due to its unique location, IZO is in the free troposphere at night (Raes et al., 1997). The MPL performed vertical profile measurements during normal ACE-2 night-time lidar operations. Several nights were very clean and the lidar returns were assumed to represent pure Rayleigh scattering with the exception of the afterpulse and overlap effects. This assumption was based on normal night-time conditions and inspection of both aerosol mass concentration and scattering and absorption coefficient measurements made at the observatory during the night. The scattering and absorption coefficients were added together to yield a value for the aerosol extinction coefficient (m^{-1}). The early mornings (00:00 GMT to 03:00 GMT) of 29 June and 15 July 1997 were chosen for calibration periods based on the low aerosol concentrations and extinction coefficients that were observed. Aerosol concentrations during the calibration periods were lower than the measurement uncertainty of $\sim 5\ \mu g/m^3$ and extinction coefficients ($\pm 5.5E\text{-}7\ m^{-1}$) were nearly an order of magnitude lower than the Rayleigh coefficient at IZO. The aerosol values are low but not zero. Therefore, some error exists in assuming a Rayleigh-only lidar signal for this calibration. Signal errors are discussed at the end of this section.

At 00:00, 01:00, 02:00, and 03:00 GMT, a 15-min average Rayleigh lidar signal, $S_R(z)$, was calculated using eq. (3) with $\beta_A(z) = 0$, E obtained from the actual time corresponding measured lidar signal, and with C set equal to 100,

$$S_R(z) = 100E\beta_R(z)\exp\left[-\frac{2}{R_R}\int_{z_L}^{z}\beta_R(z')\,dz'\right]. \quad (7)$$

The actual measured lidar signals are expressed using the following equation,

$$S_L(z) = CEO(z)\beta_R(z) \times \exp\left[-\frac{2}{R_R}\int_{z_L}^{z} \beta_R(z')\,dz'\right] + A(z), \qquad (8)$$

where $\beta_A(z)$ is still assumed to be zero. Eq. (8) can be rewritten in terms of the Rayleigh-only signal as

$$S_L(z) = O(z)S_R(z) + A(z). \qquad (9)$$

The term $S_R(z)$ is calculated and the term $S_L(z)$ is measured with the MPL system, thus the only unknowns in eq. (9) are $O(z)$ and $A(z)$. A linear regression was performed using eq. (9), the calculated Rayleigh signal, and the measured lidar signal for each altitude bin in each period (4 each night) from the chosen nights. The y intercepts where used to construct the afterpulse function and the slope was used to determine the overlap function. The resulting overlap and afterpulse functions are shown in Figs. 2a,b.

The overlap function for 29 June approaches an asymptote of almost 10, instead of the usual value of 1, as the range increases beyond 2 km. This is due to setting C equal to 100 for the calibration procedure. The actual value of C for the 29 June period was most likely much higher than 100. This is also the reason for the negative afterpulse values calculated for 29 June. The overlap and afterpulse functions for 29 June do not represent the physical overlap and afterpulse values for this period due to the arbitrary choice of C. However, the overlap and afterpulse functions still produce the correct lidar calibration. Also, the MPL crystal problems increased in magnitude as the experiment progressed, and the value of C decreased significantly. The value of C was very close to 100 by 15 July, as evidenced by the overlap asymptotic limit of approximately 1 for this day. Also, the afterpulse values for 15 July are similar to those obtained using the MPL with no crystal problem (Welton, 1998).

The average error for the measured lidar signals (at all ranges) was less than 5% during the calibration periods. Consequently, the afterpulse functions had an average error of $\sim 3\%$ or less, while the overlap functions remained unaffected by the measurement error. The overlap and afterpulse functions were used to correct MPL signals only during the days immediately after the calibration night. As an example of applying the calibration functions to the MPL data, Fig. 3 shows the original lidar signal measured at 00:00 GMT on 30 June, the calculated Rayleigh signal, and the corresponding overlap and afterpulse corrected signal. The signal now resembles a free troposphere Rayleigh-only lidar signal and demonstrates the success of the calibration procedure, despite the small amount of measurement error.

4. Analysis of ACE-2 MPL data

The MPL was operated on a daily schedule that involved vertical, horizontal, and slant path

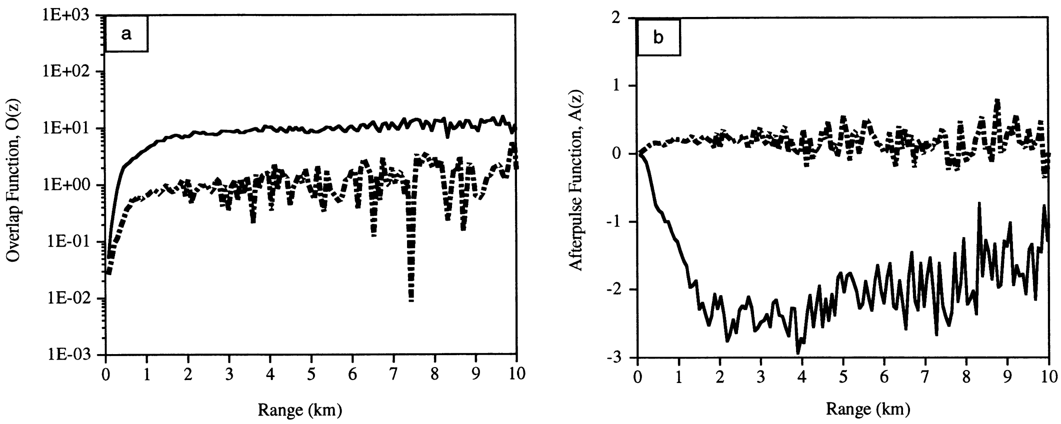

Fig. 2. (a) Overlap functions, $O(z)$, calculated on 29 June (solid line) and 15 July (dotted line) 1997. (b) Afterpulse functions, $A(z)$, calculated on 29 June (solid line) and 15 July (dotted line) 1997.

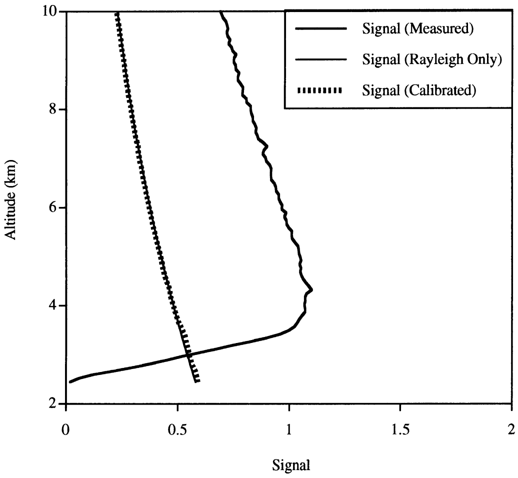

Fig. 3. The measured MPL signal, a calculated Rayleigh lidar signal, and the final calibrated MPL signal are shown for 00:00 GMT on 30 June 1997.

(T–R tilted to 60° zenith angle) measurements at specific times of the day. Vertical measurements were typically performed from 00:00 GMT to 10:30 GMT and again from 16:30 GMT to 23:59 GMT each day. Horizontal measurements were usually performed from 10:30 GMT to 11:00 GMT and from 16:00 GMT to 16:30 GMT, and slant path measurements were made each day from 11:00 GMT to 16:00 GMT. Slant path rather than vertical orientation was necessary during mid-day to prevent direct sunlight from entering the T–R and damaging the MPL detector and optics. The schedule was occasionally altered to accommodate Pelican over-flights and special ACE-2 directed activities. For this study, only vertical and selected horizontal measurements are discussed.

MPL installation and testing was performed during the first weeks and normal operation began on 28 June. The instrument problems with the MPL system became substantial after 20 July 1997 and the subsequent data resulting from the correction procedure were not considered reliable. Thus, only MPL data from 28 June to 20 July were analyzed for this study. The MPL signals were calibrated using the procedure discussed in Section 3. The signals were then divided by the lidar constant C (set equal to 100) and the corresponding output energy E. The resulting profile is referred to as an attenuated backscatter signal (ABS, units of $m^{-1}\,sr^{-1}$) because it is a profile of the total backscatter coefficient attenuated by the exponential transmission function. The ABS profiles for all the vertical measurements made from 28 June to 20 July showed that no aerosols were detected by the MPL above an altitude of approximately 6 km during ACE-2.

Most days during ACE-2 produced similar ABS profiles and were identified as the normal site condition influenced by upslope aerosols. The periods, 7 to 9 July, and 16 to 18 July, showed much higher ABS values relative to the normal site profiles and correspond to the first and second Saharan dust passages observed during ACE-2. This study will focus on the normal upslope aerosol conditions at IZO during 29 June to 1 July, and the Saharan dust episode from 16 to 18 July.

4.1. *Analysis of upslope aerosols*

During the day, local heating near IZO (along the mountain ridge) creates an upslope flow. This local wind carries aerosols from the marine boundary layer (MBL) below IZO, to the level of the observatory and beyond. The upslope aerosols appear in the early morning as the sun rises and subside by the late afternoon as the sun sets and the air temperature stabilizes. The presence of upslope aerosols during the daytime is characteristic of normal conditions at the IZO site (Raes et al., 1997), therefore, it is necessary to understand the upslope aerosol's spatial distribution and optical profile before analysis of the Saharan dust layers can be attempted.

Time series ABS profiles are shown for 29 June to 1 July in Fig. 4. The uncertainty in the ABS values (at all ranges) was less than 5% due to measurement error. Also, individual ABS profiles from early morning to late evening on 29 June are shown in Figs. 5a,b. These profiles were chosen to demonstrate the daily cycle of the upslope layers at IZO. The ABS profile at 06:15 GMT, approximately 45 min before sunrise ($\sim$07:00 GMT) is representative of a Rayleigh-only profile, no aerosol layers are present. However, the profile at 07:15 GMT shows a weak aerosol layer extending to under 6 km in altitude. The profiles at 10:15 GMT and 17:15 GMT also show aerosol layers extending to under 6 km in altitude but with much higher ABS values just over IZO. These

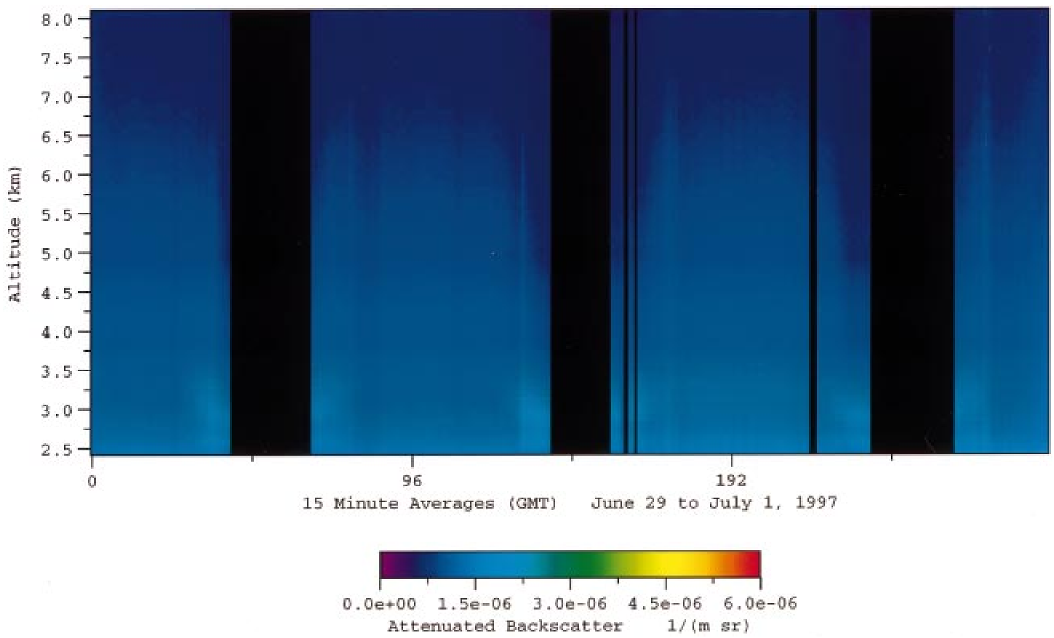

Fig. 4. 3-day attenuated backscatter signal (ABS) (m sr)$^{-1}$ time series from 29 June through 1 July 1997. ABS values have less than 5% error and each ABS profile is a 15-min average (GMT). The black gaps represent periods when the MPL was not oriented in the vertical mode.

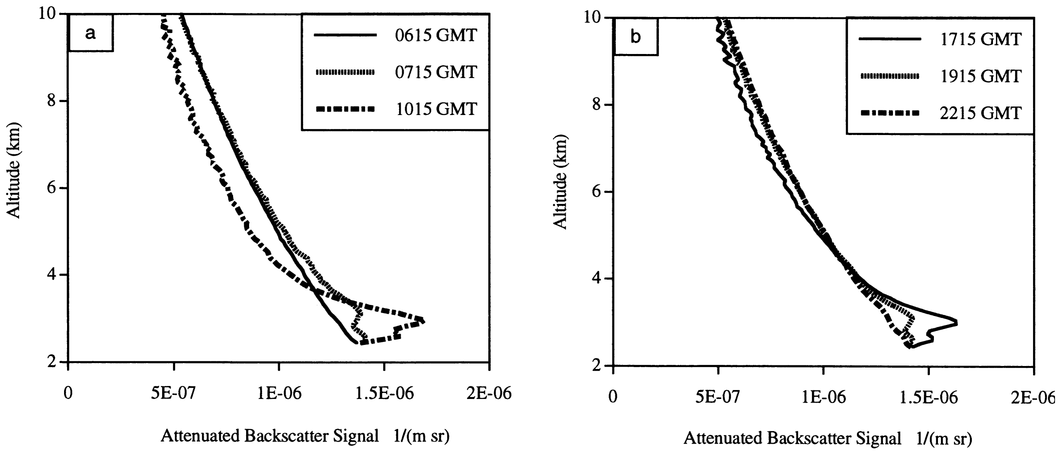

Fig. 5. (a) Attenuated backscatter signals (m sr)$^{-1}$ in the morning of 29 June 1997. (b) Attenuated backscatter signals (m sr)$^{-1}$ in the afternoon on 29 June 1997. The values have less than 5% error and each profile is a 15-min average, starting 15 min prior to the time shown.

mid-day ABS profiles are significantly less than the earlier ABS profiles at higher altitudes due to the signal attenuation by the upslope layer. The ABS profile at 19:15 GMT shows the aerosol layer subsiding, with ABS values similar to the 07:15 GMT profile, and lower than during mid-day. Finally, the ABS profile at 22:15 GMT shows no indication of aerosol layers, and instead resembles the Rayleigh-only ABS profile at 06:15 GMT. The ABS profiles in Figs. 5a,b clearly show the presence of the upslope aerosols and this pattern is typical for normal upslope conditions at IZO during ACE-2.

4.1.1. Upslope aerosol optical profiles and backscatter–extinction ratios. The AOD measured with the IZO Cimel was used to calculate the R_A, and profiles of the aerosol extinction coefficient (AEC) and AOD for the upslope aerosol layers on 29 June 1997 using the inversion algorithm discussed in Section 7. The profiles analyzed for 29 June are representative of normal upslope aerosol conditions during ACE-2 and were chosen to coincide with Cimel measurements of the AOD. The Cimel AOD was ~ 0.01 AOD units, and agrees well with the AOD measured by the Teide shadowband. The AOD of the upslope layer is very small and is equal to the measurement uncertainty of both instruments (± 0.01 AOD units). The low AOD values measured by the instruments demonstrate the absence of Saharan dust during this period.

The AEC and AOD profiles each correspond to a calculated columnar R_A value from the lidar inversion. The R_A values for the upslope aerosol profiles averaged $0.026\ sr^{-1}$. Error in the BER from the lidar measurement uncertainty was 3%. However, BER errors resulting from uncertainty of the measured Cimel AOD were near 50% due to the extremely low AOD of the upslope layer. Therefore, the uncertainty in the BER for the upslope aerosol layer is $\pm 0.013\ sr^{-1}$. Low R_A values ($\sim 0.020\ sr^{-1}$) during the early morning and late afternoon, and higher R_A values ($\sim 0.035\ sr^{-1}$) during mid-day were characteristic of upslope aerosol conditions at IZO during ACE-2.

The large amount of uncertainty in the BER (due to low aerosol concentrations) makes determination of the AEC extremely difficult. Variation in the AEC and AOD values of the profiles averaged $\sim 2\%$ or less from measurement uncertainty of the lidar. However, the total error in the AEC and AOD is very large due to the low concentrations and further analysis of the upslope aerosol optical profiles is not feasible.

4.1.2. Upslope horizontal lidar signal results. Horizontal lidar measurements (approximately due East) during upslope conditions were performed. The natural logarithm of the horizontal ABS at 10:45 GMT on 29 June is shown in Fig. 6 along with a calculated Rayleigh horizontal plot. The presence of the upslope aerosols along the side of the mountain is shown by the elevated and non-linear ABS values out to approximately 1.5 km from the side of the mountain. The plot becomes linear after 1.5 km, thus, the atmosphere does appear to be horizontally homogeneous from 1.5 km out to 6 km (the maximum daytime range of the MPL during most of ACE-2). However, near the side of the mountain, and near IZO, the presence of upslope aerosols results in horizontal inhomogeneity.

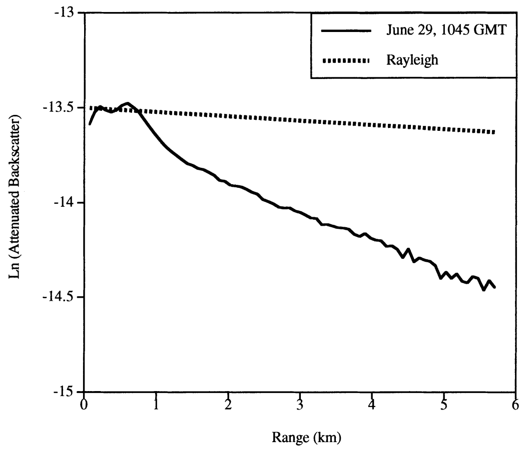

Fig. 6. Horizontal lidar profile of the natural logarithm of the attenuated backscatter signal (ABS) (m sr)$^{-1}$. ABS values have less than 5% error. A 15-min average horizontal profile at 10:45 GMT on 29 June is shown along with a calculated Rayleigh horizontal profile for the IZO altitude.

4.2. *Analysis of Saharan dust episode*

Three Saharan dust episodes occurred during ACE-2. Each episode was characterized by the presence of dust layers at and above the IZO site. The first dust episode started at mid-day on 7 July and continued until the afternoon of 9 July. The second dust episode started late in the evening on 16 July and continued until the morning of 18 July. The last dust episode started on the morning of 25 July and continued into 26 July, past the end of ACE-2.

During much of the first dust episode, the MPL was orientated in the slant path position. During this episode, inspection of the dust layer lidar returns and IZO aerosol concentration and nephelometer data showed that very little of the dust was at the IZO altitude. The decision was made to orient the MPL on a slant path in order to attempt to measure dust below the lowest vertical measurement range (75 m) of the MPL. As a result, there is little vertical MPL data during the first dust episode. The last dust episode occurred after the period when the MPL data could be accurately corrected. The results presented below for Saharan dust layers are derived from analysis performed on data acquired during the second dust episode, from 16 to 18 July.

It is important to note that sulfates and other aerosol species have often been correlated with dust episodes at IZO and elsewhere over the North Atlantic Ocean (Welton et al., unpublished data; Maring, personal communication). Therefore, the results presented in this section for dust conditions at IZO are likely to include some effects from aerosols other than dust, and may in fact underestimate the effects of the dust aerosols alone.

A time series of ABS profiles from 16 through 18 July is shown in Fig. 7. The uncertainty in the ABS values (at all ranges) averaged ~5% due to measurement error. The temporal extent of the dust layer is clearly evident. The dust layer appeared at approximately 22:00 GMT on 16 July at an altitude of approximately 3.5 km. The layer dropped in altitude by the morning of 17 July with the majority of the dust at altitudes from about 2.5 km to about 4 km until the late afternoon. The layer thickness narrowed in altitude considerably after 18:00 GMT on 17 July. Most of the dust remained at altitudes from about 2.75 km to 3.5 km for the duration of the episode, which ended the morning of 18 July.

4.2.1. Dust aerosol optical depth profiles and backscatter–extinction ratios. The AOD measured with the IZO Cimel was used to calculate R_A, and the AEC and AOD profiles for the dust layers on 17 July 1997 using the lidar inversion algorithm discussed in Section 7. The lidar AEC profiles calculated throughout the day (08:15, 10:15, 17:15, and 18:45 GMT) on 17 July are shown in Fig. 8 along with the Rayleigh extinction coefficient profile for comparison. The average AEC uncertainty (for values at all ranges) was ~7%. The profiles at 10:15 and 17:15 GMT had slightly

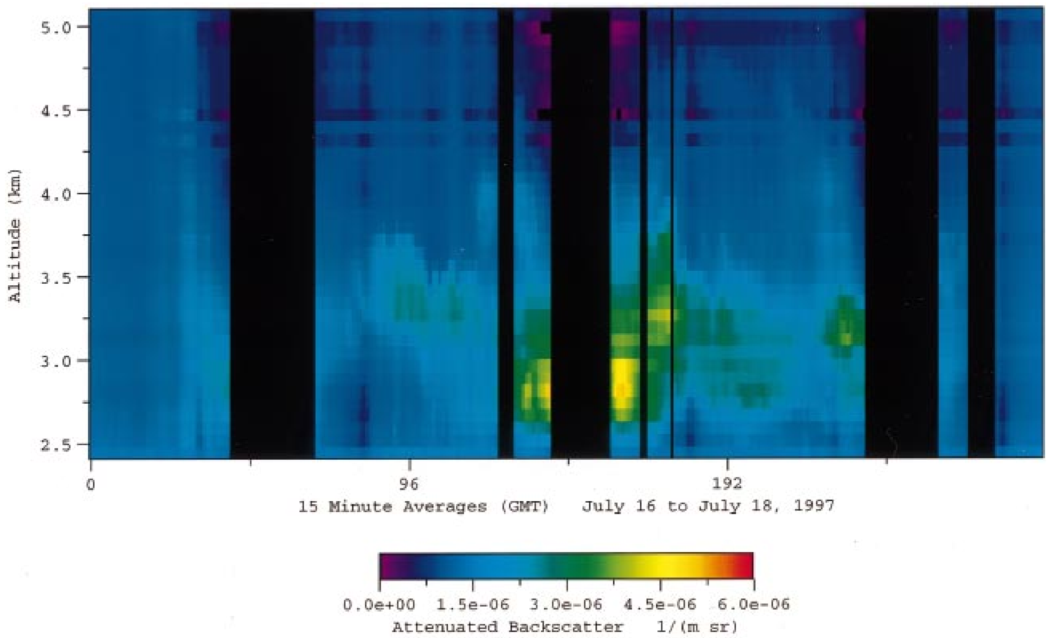

Fig. 7. 3-day attenuated backscatter signal (ABS) (m sr)$^{-1}$ time series from 16 through 18 July 1997. ABS values have an average error of 5% and each ABS profile is a 15-min average (GMT). The black gaps represent periods when the MPL was not oriented in the vertical mode.

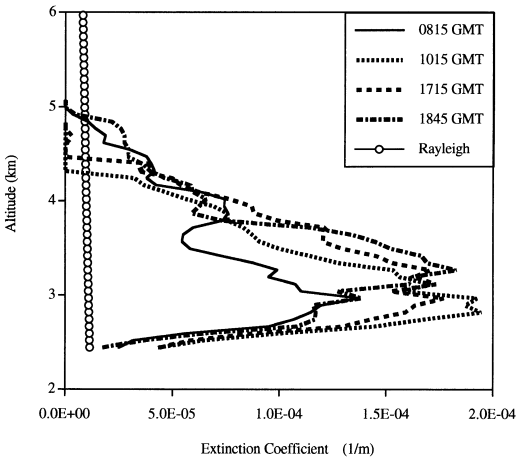

Fig. 8. Lidar aerosol extinction coefficient (m^{-1}) profiles ($\sim 7\%$ error) at 08:15, 10:15, 17:15, and 18:45 GMT on 17 July 1997. The columnar AOD (± 0.01) for each profile is 0.161, 0.205, 0.226, and 0.217 respectively. The calculated columnar backscatter–extinction ratios (sr^{-1}) for each profile are 0.026 ± 0.007, 0.048 ± 0.012, 0.073 ± 0.018, and 0.027 ± 0.007 respectively. The Rayleigh extinction coefficient profile is shown for comparison.

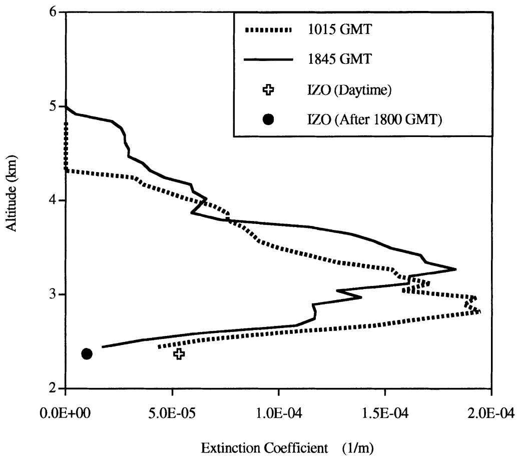

Fig. 9. Lidar aerosol extinction coefficient (m^{-1}) profiles ($\sim 7\%$ error) at 10:15 and 18:45 GMT on 17 July 1997. The columnar AOD (± 0.01) for each profile is 0.205 and 0.217 respectively. The calculated columnar backscatter–extinction ratios (sr^{-1}) for each profile are 0.048 ± 0.012 and 0.027 ± 0.007 respectively. The average aerosol extinction coefficients obtained at IZO ($\pm$5.5E-7) from 07:00 to 18:00 GMT (daytime) and after 18:00 GMT are also shown.

larger errors due to a drop in the signal-to-noise ratio during mid-day. This was caused by the combination of increased background sunlight during the day and high signal attenuation by the dust layer. The results from the 08:15 and 18:45 GMT profiles were not as affected by this problem and the results from these periods are more reliable.

The lidar R_A values calculated for the 08:15, 10:15, 17:15, and 18:45 GMT profiles were 0.026, 0.048, 0.073, and 0.027 sr^{-1}, respectively. The error in the BER was 25% for these profiles, much lower than the upslope aerosol case. This error was caused primarily by the lidar measurement uncertainty and not the Cimel AOD uncertainty (± 0.01), opposite to the upslope aerosol case. In general, the R_A increased during mid-day (average $\sim 0.06\ sr^{-1}$) compared to R_A values for morning and late afternoon (average $\sim 0.027\ sr^{-1}$). However, the mid-day R_A values may be inaccurate due to the noise problem discussed above. Therefore, the BER for the dust layer is $0.027 \pm 0.007\ sr^{-1}$ (obtained from the morning and late afternoon profiles only).

Fig. 9 shows the 17 July lidar AEC profiles at 10:15 and 18:45 GMT along with the Rayleigh extinction coefficient profile for comparison. Fig. 9 also shows the average AEC measured at IZO (uncertainty $\pm 5.5e\text{-}7\ m^{-1}$) for both mid-day (daytime) and after 18:00 GMT. The lidar AEC values at 2.442 km agree well with the IZO AEC values. The peak lidar AEC values were between $1.5e\text{-}4$ and $2e\text{-}4\ m^{-1}$ and were located just above 3 km in altitude. Significant AEC values (greater than the Rayleigh extinction coefficient) were present from the IZO altitude to just under 5 km.

Fig. 10 shows the lidar AOD profile at 18:45 GMT. The uncertainty in lidar AOD values averaged 6% for all ranges (average ± 0.013 AOD units). Fig. 10 also shows the AATS-14 AOD profile from 18:30 to 18:45 GMT, and the AOD measured by the Teide shadowband and the IZO Cimel for this time period. The uncertainty in AOD for these other instruments was ± 0.01 AOD units or less. The AATS-14 AOD values immediately above the IZO altitude (within 100 m over the observatory), average 0.218 ± 0.05 AOD units. This portion of the Pelican flight corresponds to horizontal flight tracks across the mountain ridge, approximately 50 m over IZO. The spread in

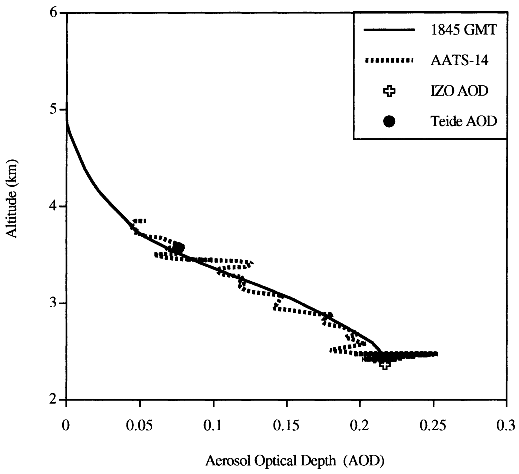

Fig. 10. Lidar aerosol optical depth (AOD) profile (average error ± 0.013) at 18:45 GMT on 17 July 1997 (solid line). The calculated columnar backscatter–extinction ratio (sr^{-1}) is 0.027 ± 0.007. The AOD profile measured with AATS-14 from 18:30 to 18:45 GMT, and the AOD measured by the IZO Cimel and the Teide shadowband, are also shown. Errors in the AOD from the other instruments are ± 0.01 or less.

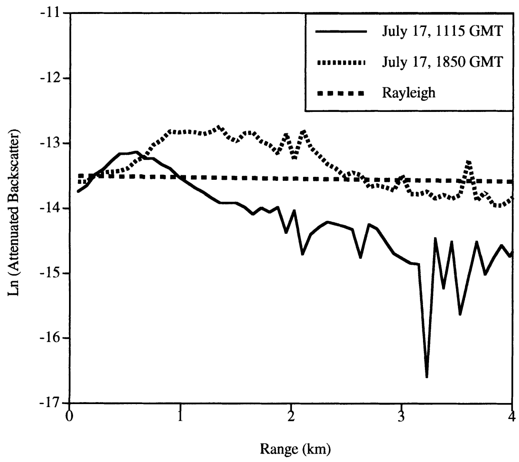

Fig. 11. Horizontal lidar profiles of the natural logarithm of the attenuated backscatter signal $(m\ sr)^{-1}$. ABS values have an average of 5% error. A 15-min average horizontal profile at 11:15 GMT and a 5-min average horizontal profile at 18:50 GMT on 17 July are shown along with a calculated Rayleigh horizontal profile for the IZO altitude.

AOD (± 0.05) for these tracks is evidence of slight changes in the horizontal homogeneity of the dust layer overhead. The AOD values from all instruments agree within instrumental uncertainties for most of the profile and they agree better than the ± 0.05 AOD spread from horizontal inhomogeneity for the entire profile. The excellent agreement between the lidar data and the data from the other instruments for this time shows that the MPL calibrations and inversion algorithm worked successfully and that the R_A calculated for this dust episode was accurate.

4.2.2. Dust horizontal lidar signal results. Horizontal profiles (lidar aimed approximately due East) of the natural logarithm of the ABS on 17 July at 11:15 and 18:50 GMT are shown in Fig. 11, along with a calculated Rayleigh profile for comparison. Both measured lidar profiles are non-linear within 2 km of IZO, indicating that horizontal homogeneity did not exist near the mountain ridge. The 11:15 GMT plot appears to be fairly linear (but noisy) from 1.5 to 4 km, and the 18:50 GMT plot is linear from 2.5 to 4 km. Therefore, the atmosphere does appear to be horizontally homogeneous from approximately 2 km to 4 km (the maximum horizontal range with dust present) away from the mountain ridge during this dust episode.

The sharply increasing ABS within the first kilometer of range for the 11:15 GMT plot shows that a large amount of aerosol was present within 1 km from the ridge relative to the situation at 18:50 GMT. The increase in aerosol within 1 km of the ridge during daytime (11:15 GMT) corresponds to the upslope period. The 18:50 GMT profile shows that less aerosol was located close to the mountain side (within 1 km), and corresponds to the period after the upslope has subsided ($\sim$18:00 GMT). The upslope wind motion appears to have changed the dust layer near the mountain and indicates the importance of considering upslope effects on the horizontal homogeneity of the region around IZO.

5. Conclusions

The operation of the MPL system during ACE-2 has shown that this new lidar technology can be used successfully in the field. ACE-2 closure comparisons between the MPL system and other independently operated instruments have shown that the MPL calibration procedures and inversion algorithm succeed in producing accurate optical profiles throughout the entire range of the profile. This is significant because it shows that the overlap and afterpulse problems can be overcome, even when the MPL has suffered an instrument problem.

The results of lidar analysis during ACE-2 have shown several interesting characteristics of the upslope aerosols and the Saharan dust episode during the middle of the experiment. The upslope aerosols were seen to form a layer several hundred meters above and to the sides of IZO during the day, and to subside by nightfall. The dust layer on 17 July was seen to reside mostly above and to the sides of IZO, possibly held off by the motion of upslope winds despite findings that show upslope winds to be weaker during dust episodes (Raes et al., 1997). The possible perturbation of the dust layer by the upslope effect is significant in view of the fact that the IZO site is used during summer months to study Saharan dust layers. Peak AEC values obtained during the dust episode were an order of magnitude higher than Rayleigh values. The dust layer altitude ranges observed during ACE-2 (from just over 2 km to under 5 km) correspond well with other investigations of the vertical structure of the Saharan air layer (SAL) over the North Atlantic Ocean (Carlson and Prospero, 1972; Karyampudi and Carlson, 1988). Another important result was the determination of an accurate R_A value ($0.027 \pm 0.007\ \mathrm{sr}^{-1}$) for the dust episode on 17 July.

Results from an MPL located in Las Galletas (Tenerife) during ACE-2 are reported in Powell et al. (this issue). Las Galletas is at sea level and on the southern tip of the island. They report an AOD of 0.250 ± 0.050 for the dust layer. The AOD measured by all instruments discussed in this study agree with the Las Galletas value within the uncertainty due to horizontal homogeneity (± 0.05, as estimated from the Pelican horizontal track over IZO on 17 July). Furthermore, Powell et al. report the peak dust AEC to be $\sim 1.7e\text{-}4\ \mathrm{m}^{-1}$ at an altitude of approximately 3 km. This agrees well with our reported peak AEC values of $1.5e\text{-}4$ to $2e\text{-}4\ \mathrm{m}^{-1}$ at an altitude just over 3 km. Finally, Powell et al. determine a value of $0.029 + 0.004\ \mathrm{sr}^{-1}$ for the dust R_A value. This agrees within experimental uncertainty to our R_A value of $0.027 + 0.007\ \mathrm{sr}^{-1}$. Knowledge of an accurate R_A during dust episodes will aid in the analysis of future lidar measurements in regions influenced by dust aerosols.

6. Acknowledgements

This research is a contribution to the International Global Atmospheric Chemistry (IGAC) core project of the International Geosphere-Biosphere Programme (IGBP) and is part of the IGAC Aerosol Characterization Experiments (ACE). The authors extend great appreciation to E. Cuevas, R. Juega Buide, and the rest of the Izaña observatory staff for their support during ACE-2. Thanks is also given to A. Chapin for invaluable work in preparing the micro-pulse lidar system for field use. MPL measurements during ACE-2 were funded by NASA contract #NA55-31363. Funding for the measurements and analyses presented in this work was provided by the National Aeronautics and Space Administration, US National Science Foundation, Office of Naval Research, European Commission DG XII (Environment and Climate), Max Planck Society, and the National Oceanic and Atmospheric Administration.

7. Appendix A

The lidar inversion algorithm

The lidar inversion algorithm used for this study is presented in this section. Also, errors inherent to the algorithm are discussed. The primary error is due to the assumption of a constant backscatter–extinction value, R_A.

7.1. *Solution to the lidar equation*

The $\beta_A(z)$ solution to lidar data taken according to eq. (3) is referred to as the backward Fernald 2-component solution (Fernald et al., 1972). The solution uses the value of the backscattering coefficient at some maximum altitude, z_m, as a boundary value and then successive values of $\beta_A(z)$ are calculated as the altitude is decreased toward the lidar altitude, z_L. The solution can be written as (Fernald, 1984):

$$\beta_A(x-1) = \frac{S_r(x-1)\Psi(x-1,x)}{\dfrac{S_r(x)}{\beta_A(x)+\beta_R(x)} + \dfrac{1}{R_A}[S_r(x)+S_r(x-1)\Psi(x-1,x)]\Delta z} - \beta_R(x-1), \quad \text{(A.1)}$$

where

$$\Psi(x-1,x) = \exp\left[\left(\frac{1}{R_A}-\frac{1}{R_R}\right) \times (\beta_R(x-1)+\beta_R(x))\Delta z\right], \quad \text{(A.2)}$$

and x is the altitude bin one step above $x-1$, and Δz is the lidar range interval (75 m). In order to obtain the extinction coefficient profile, each value of the backscattering coefficient need only be divided by R_A.

The basic lidar algorithm that uses eq. (A.1) to solve for the aerosol profiles must assume that R_A and the backscattering coefficient at some maximum altitude, $\beta_A(z_m)$, are known. R_A is not usually known, but the latter constraint is usually valid as aerosols are normally confined to the marine boundary layer (MBL), or at least at low altitudes above the lidar (such as over IZO), therefore, z_m can be chosen at an altitude where $\beta_A(z_m)=0$. An algorithm was developed for this study that uses an independently measured AOD, τ_A, to constrain R_A and produce a σ_A profile that integrates to the measured AOD.

7.2. *Lidar inversion algorithm*

This algorithm is based on procedures described in Fernald et al. (1972) and Marenco et al. (1997). The algorithm produces extinction coefficient and AOD profiles, and also calculates R_A. The algorithm is described below and presented schematically in Fig. 12.

The first step in the algorithm requires determination of β_A at some maximum altitude, z_m, and is done by inspection of the calibrated signals. Inspection of the signals obtained during ACE-2 showed that no aerosol appeared to be present ($\beta_A \sim 0$) above a maximum altitude, and z_m was chosen to lie just above this altitude, with β_A set equal to 0.

The second step in the algorithm is the calculation of β_A one altitude step, 75 m, below z_m. This is done by solving eq. (A.1) with $\beta_A(x=z_m)=0$, and the Rayleigh profile quantities; $\beta_R(z)$, $\sigma_R(z)$, and R_R, from Hansen and Travis (1974). For the first step in the algorithm, R_A is set equal to 1

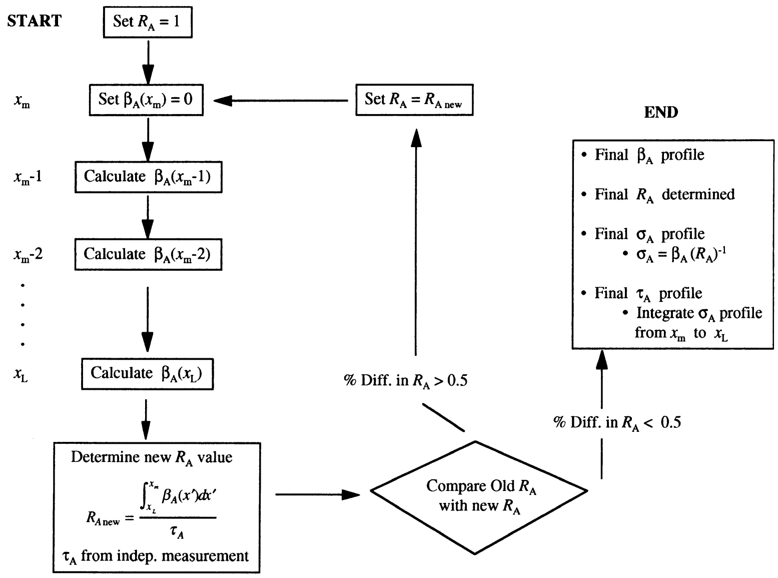

Fig. 12. Schematic representation of the lidar inversion algorithm.

and $\beta_A(x-1)$ is calculated. This process is repeated downward through the atmosphere, with $R_A = 1$ and $\beta_A(x+1)$ obtained from the previous step, until the value of β_A is calculated at the lowest altitude bin (75 m above the MPL system altitude).

The next step in the algorithm is to improve the estimate of R_A (determination of $R_{A\,\mathrm{new}}$). $R_{A\,\mathrm{new}}$ is determined using the backscattering coefficient profile calculated in the previous step (with $R_A = 1$) and the following equation,

$$R_{A\,\mathrm{new}} = \frac{\int_{z_L}^{z_m} \beta_A(z')\,\mathrm{d}z'}{\tau_A}, \tag{A.3}$$

with τ_A from the independent AOD measurement. The backscattering coefficient profile is now recalculated, using $\beta_A(x = z_m) = 0$, but with $R_A = R_{A\,\mathrm{new}}$. This process is continued until successive values of R_A and $R_{A\,\mathrm{new}}$ differ negligibly (the difference between R_A and $R_{A\,\mathrm{new}}$ is less than 0.5%). The final backscattering coefficient profile and R_A are then used to calculate the extinction coefficient profile, $\sigma_A(z)$. The extinction coefficient profile is then numerically integrated from z_L to z_m, and then subtracted from τ_A at each altitude step, to produce an AOD profile, $\tau_A(z)$. Thus the final data products from the algorithm are the extinction coefficient and AOD profiles and R_A.

7.3. *Errors in the results from the lidar inversion algorithm*

This algorithm was tested with artificial lidar data to study the effects of errors caused by the algorithm and the assumption of a constant R_A (Welton, 1998). Both a single and a 2 aerosol species atmosphere were tested. The results show that in a single aerosol species atmosphere (with constant R_A) the algorithm accurately calculates the $\beta_A(z)$ profile and the correct R_A (and thus accurate $\sigma_A(z)$ and AOD profiles) even if the concentration of the aerosols varies vertically and the aerosols are separated into different layers. For cases with 2 aerosol species (different R_A values and backscattering coefficient profiles), the results show that the algorithm was found to calculate an R_A value that was an accurate average of the 2 different R_A values when the species were in one continuous layer (but not mixed together) or separated into 2 distinct layers. For real situations, different aerosol species are often mixed together and it is expected that the final R_A calculated will be dependent more on the relative amounts of each aerosol and will not produce a direct average of the different individual R_A values. However, the algorithm will produce an accurate columnar value of the R_A in real situations. This is an important result since other ground-based instruments that measure R_A related quantities, such as the aerosol phase function, also measure the entire atmospheric column.

Errors were present in the resulting $\beta_A(z)$ profiles when the constant R_A inversion algorithm was applied to an inhomogeneous R_A atmosphere. The initial $\beta_A(z)$ profile values near z_m are correct but successive values of β_A deviate from the correct value. This fact and the calculation of an average R_A influences the calculation of the $\sigma_A(z)$ profile. The algorithm will force the final $\sigma_A(z)$ profile to integrate to the correct τ_A value. The value, β_A/R_A, will be iterated continually, until the correct τ_A value is reached. If the R_A value used is incorrect, then the resulting β_A profile will have errors.

These types of R_A related errors have been studied by other researchers in depth (Klett, 1985; Sasano et al., 1985; Kovalev, 1993; Kovalev and Moosmuller, 1994). In order to attempt to overcome errors associated with the choice of a constant R_A, these researchers have constructed algorithms using range dependent R_A values. However, for these algorithms an R_A profile, from modeled or independent data, must be used. The choice was made to use a constant R_A algorithm for this study since neither data, nor models of R_A, were available during the lidar campaigns.

REFERENCES

Carlson, T. N. and Prospero, J. M. 1972. The large-scale movement of Saharan air outbreaks over the Northern Equatorial Atlantic. *J. Appl. Meteorol.* **11**, 283–297.

Fernald, F. G. 1984. Analysis of atmospheric lidar observations: some comments. *Appl. Optics* **23**, 652–653.

Fernald, F. G., Herman, B. M. and Reagan, J. A. 1972. Determination of aerosol height distributions by lidar. *J. Appl. Meteorol.* **11**, 482–489.

Formenti, P., Andreae, M. O. and Lelieveld, J. 2000. Measurements of aerosol optical depths in the North Atlantic free troposphere: results from ACE-2. *Tellus* **52B**, 676–693.

Hansen, J. E. and Travis, L. D. 1974. Light scattering in planetary atmospheres. *Space Sci. Reviews* **16**, 527–610.

Holben, B. N., Eck, T. F., Slutsker, I., Tanre, D., Buis, J. P., Setzer, A., Vermote, E., Reagan, J. A., Kaufman, Y. J., Nakajima, T., Lavenu, F., Jankowiak, I. and Smirnov, A. 1998. AERONET-A federated instrument network and data archive for aerosol characterization. *Rem. Sens. Environ.* **66**, 1–16.

Karyampudi, V. M. and Carlson, T. N. 1988. Analysis and numerical simulations of the Saharan Air Layer and its effects on easterly wave distrubances. *J. Atmos. Sci.* **45**, 3102–3136.

Klett, J. D. 1985. Lidar inversion with variable backscatter/extinction ratios. *Appl. Optics* **24**, 1638–1643.

Kovalev, V. A. 1993. Lidar measurement of the vertical aerosol extinction profiles with range-dependent backscatter-to-extinction ratios. *Appl. Optics* **32**, 6053–6065.

Kovalev, V. A. and Moosmuller, H. 1994. Distortion of particulate extinction profiles measured with lidar in a two-component atmosphere. *Appl. Optics* **33**, 6499–6507.

Marenco, F., Santacesaria, V., Bais, A. F., Balis, D., Di Sarra, A., Papayannis, A. and Zerefos, C. 1997. Optical properties of tropospheric aerosols determined by lidar and spectrophotometric measurements (Photochemical Activity and Solar Ultraviolet Radiation campaign). *Appl. Optics* **36**, 6875–6886.

Prospero, J. M., Schmitt, R., Cuevas, E., Savoie, D., Graustein, W., Turekian, K., Volz-Thomas, A., Oltmans, S., Levy, H. and Diaz, A. 1995. Temporal variability of ozone and aerosols in the free troposphere over the Eastern North Atlantic. *Geophys. Res. Lett.* **22**, 2925–2928.

Raes, F., Bates, T. S., McGovern, F. M. and Van Liedekerke, M. 2000. The second Aerosol Characterization Experiment (ACE-2): general overview and main results. *Tellus* **52B**, 111–126.

Raes, F., Van Dingenen, R., Cuevas, E., Van Velthoven, P. F. J. and Prospero, J. M. 1997. Observations of aerosols in the free troposphere and marine boundary layer of the subtropical Northeast Atlantic: discussion of processes determining their size distribution. *J. Geophys. Res.* **102**, 21,315–21,328.

Russell, P. B. and Heintzenberg, J. 2000. An overview of the ACE 2 Clear Sky Column Closure Experiment (CLEARCOLUMN). *Tellus* **52B**, 463–483.

Sasano, Y., Browell, E. V. and Ismail, S. 1985. Error caused by using a constant extinction/backscattering ratio in the lidar solution. *Appl. Optics* **24**, 3929–3932.

Schmid, B., Livingston, J. M., Russell, P. B., Durkee, P. A., Jonsson, H. H., Collins, D. R., Flagan, R. C., Seinfeld, J. H., Gassó, S., Hegg, D. A., Öström, E., Noone, K. J., Welton, E. J., Voss, K. J., Gordon, H. R., Formenti, P. and Andreae, M. O. 2000. Clear sky closure studies of lower tropospheric aerosol and water vapor during ACE-2 using airborne sunphotometer, airborne in-situ, space-borne, and ground-based measurements. *Tellus* **52B**, 568–593.

Smirnov, A., Holben, B. N., Slutsker, I., Welton, E. J. and Formenti, P. 1998. Optical properties of Saharan dust during ACE-2. *J. Geophys. Res.* **103**, 28,079–28,092.

Spinhirne, J. D. 1993. Micro pulse lidar. *IEEE Trans. Geosci. Remote Sens.* **31**, 48–55.

Spinhirne, J. D., Rall, J. and Scott, V. S. 1995. Compact eye-safe lidar systems. *Rev. Laser Eng.* **23**, 26–32.

Welton, E. J. 1998. *Measurements of aerosol optical properties over the ocean using sunphotometry and lidar*. PhD Dissertation. University of Miami, Coral Gables, 1–150.